RSC Advances

PAPER

View Article Online
View Journal | View Issue

Cite this: *RSC Adv.*, 2026, **16**, 17860

Potential screening of oral squamous cell carcinoma using microRNA geno-assay by electrochemical sensing: a new platform in biosensor technology

Hamed Bahari,[ab] Mohammad Hasanzadeh,*[a] Soodabeh Davaran,*[c] Farzin Ahmadpour,[d] Fereshteh Kohansal[e] and Nasrin Shadjou[f]

Early-stage diagnosis of oral squamous cell carcinoma (OSCC), a prominent global cause of mortality, is crucial for minimizing morbidity and mortality rates. MicroRNA-423-5p is chosen for effective identification of OSCC because of its high specificity in the Receiver Operating Characteristic (ROC) curve, enabling precise diagnosis of oral cancer (OC) in human biofluids. This work introduces a novel label-free electrochemical platform for the non-invasive recognition of microRNA-423-5p in human saliva samples. The monitoring is achieved by a DNA-based bioassay. In order to achieve this objective, polychitosan (P(CS)) was electropolymerized on the surface of a glassy carbon electrode (GCE) and used as a high-potential capturing layer on the surface of the GCE. Also, triangular silver nanoparticles (TA-AgNPs) were used for stable immobilization of probe-DNA. This allowed for the effective immobilization of thiolated DNA sequences *via* the interaction with TA-AgNPs. This immobilization was achieved utilizing a DNA-microRNA-423-5p hybridization approach. Therefore, a label-free genosensor was prepared for the sensitive recognition of OC. Using the electroanalysis method, microRNA-423-5p was determined in human saliva samples in the linear range of 1pM to 5 nM with a low limit of quantification of 1 pM. Because this report is the first application of electroanalysis strategy to the recognition of OC biomarker (microRNA-423-5p), therefore, a new horizon opens for cancer diagnosis.

Received 19th September 2025
Accepted 1st March 2026

DOI: 10.1039/d5ra07098h

rsc.li/rsc-advances

1 Introduction

Malignant neoplasm in the lips, oral cavity, and oropharynx area is the exact classification for oral and oropharyngeal cancer. The definition of the related risk factors is significantly influenced by geographic and environmental factors.[1] Head and neck cancer (HNC) ranks as the sixth most prevalent form of cancer globally.[2] Oral squamous cell carcinoma (OSCC) is the prevailing malignant neoplasm affecting the oral and maxillofacial areas. A contributing factor to the poor five-year survival rates of OSCC is the diagnostic delay.[3] In the first stages, the five-year survival rate exceeds 80%, but it drops to less than 30% for advanced illness.[4] Over 60% of oral OSCCs are detected at a late stage, resulting in significant illness and death rates.[4] The occurrence and death rates emphasize the significance of oral cancer (OC) screening initiatives in enhancing timely identification and treatment effectiveness.[4] Nevertheless, literature review indicates that OSCC may also develop from epithelium that doesn't seem to be dysplastic. These lesions have a delicate histology that makes underdiagnosis easy. Specifically, it was recently shown by examination of the anomalies in the mucosa around OSCC that the dysplastic alterations are often mild (70%, exhibiting characteristics of differentiated dysplasia), and as such, the pathologist may easily underappreciate them.[5]

The conventional method of visually examining oral (VOE)[6–8] lesions may effectively monitor patient mortality when they are exposed to risk factors. Nevertheless, there are some drawbacks that restrict the use of these methods in a clinical setting. Therefore, the use of screening tools that effectively distinguish between a non-cancerous and cancerous abnormality, while also providing information regarding early OSCC, may improve the outcomes and reduce the difficulties associated with diagnosing of OC.[9] Tissue-fluorescence imaging[10–12] and optical coherence tomography[11,12] have shown significant efficacy as of late in the field of optical imaging technologies.[9] Furthermore,

[a]*Pharmaceutical Analysis Research Center, Pharmaceutical Sciences Institute, Tabriz University of Medical Science, Tabriz, Iran. E-mail: hasanzadehm@tbzmed.ac.ir*
[b]*Research Center for Pharmaceutical Nanotechnology, Pharmaceutical Sciences Institute, Tabriz University of Medical Science, Tabriz, Iran*
[c]*Department of Medical Nanotechnology, Faculty of Advanced Medical Sciences, Tabriz University of Medical Sciences, Tabriz, 516661-4733, Iran. E-mail: davaran@tbzmed.ac.ir*
[d]*Department of Oral and Maxillofacial Surgery, Dentistry Faculty, Tabriz University of Medical Sciences, Tabriz, Iran*
[e]*Drug Applied Research Center, Tabriz University of Medical Science, Tabriz, Iran*
[f]*Department of Nanotechnology, Faculty of Chemistry, Urmia University, Urmia, Iran*

there has been a significant focus on conducting thorough investigations into the use of nanoparticles for DNA analysis and salivary proteomics. Nevertheless, the absence of adequate clinical studies and the lack of association with biopsy results impede the use of these screening tools in medical clinics.[9]

Only around 2 percent of the human genome's sequence is thought to be made up of the roughly 20 000 protein-coding genes. Conversely, non-coding RNA (ncRNAs) refers to the remaining approximately 3000 genes, which are only translated into RNA and do not encode proteins.[13] Noncoding RNAs, including microRNA (miRNA),[14] long noncoding RNA (lncRNA),[15] small nucleolar RNA (snoRNA),[16] Circular RNA (circRNA),[17] and Piwi-interacting RNA (pi-RNA),[18] have a role in controlling cell proliferation, promoting migration and invasion, preventing cell death, and activating resistance to chemotherapy. Identifying these abnormal non-coding RNAs in biological specimens (such as tumor tissue, blood, and saliva) might aid in the detection, prediction, and management of OC.[2,19,20]

The words "salivaomics"[21] were first used in 2008 to highlight the several "omics" that are present in saliva, including the microbiome,[22,23] transcriptome,[24,25] proteome,[26,27] and genome. The development of more sophisticated analytical methods has allowed salivaomics to be extensively researched in recent years. Saliva contains around 70% human DNA, with the remaining 30% being made up of oral microbiota. Saliva has around 24 μg of DNA (range 0.2 to 52 μg), which is about ten times less than blood, however genotyping methods may function with as little as 5 ng mL^{-1} of DNA.[28] It has long been a goal but has not yet been achieved to utilize saliva for the diagnosis of OC.[29] According to recent research, salivary proteins and cell-free mRNAs may be used to diagnose systemic disorders like mouth cancer. Saliva is thus a significant diagnostic fluid and provides the possibility of the diagnosis of illness in a non-invasive[30] and specific way thanks to the development of highly sensitive and precise test for salivary mRNA and protein biomarkers. Saliva provides a number of benefits, including simpler collection, less expensive storage, and simpler transportation. Furthermore, the non-invasive saliva-based ways of collecting samples may significantly reduce patient pain and anxiety while assessing their overall health and illness.[29]

Based on the previous reports, the high level beneath the chart in the Receiver Operating Characteristic (ROC) curve led to the selection of microRNA-423-5p as a diagnostic biomarker of OC.[31] ROC plot combines specificity and sensitivity into a single image that allows researchers to assess the accuracy of several indicators graphically.[32] Saliva samples were taken from patients with OSCC and newly identified untreated primary healthy controls. Salivary miRNAs were profiled worldwide using a microarray technique, and the signatures were confirmed using quantitative real-time PCR (RT-qPCR).[31] Twenty-five miRNAs showed differential expression in OSCC patients and healthy controls; seven of them were shown to be significantly correlated with disease-free survival (DFS).[31] Significant expression levels of miR-423-5p, miR-193b-3p, and miR-106b-5p were found in the saliva of OSCC patients, and their combination shows the best diagnostic effectiveness (ROC − AUC = 0.98). Furthermore, when included in a multivariate survival analysis with the number of positive lymph nodes-the only relevant clinical prognosticator-strong expression of microR-423-5p was an independent predictor of poor DFS. Therefore, microR-423-5p is found to be a suitable biomarker for identifying OC by patient saliva sample analysis.[31]

Till now different biosensors were used to early-stage diagnosis of OC using detecting certain biomarkers present in saliva. But there is no report on the application of biosensor technology towards identification of OC by monitoring of MicroRNA-423-5p in human saliva samples. In this study we wanted to introduce the first biosensor for the non-invasive screening of OC in human real samples. This research work introduces a pioneering electrochemical label-free biosensor, the first of its kind in the field, offering a transformative perspective on early-stage diagnosis of OC. To the best of our knowledge, no biosensor has yet been created expressly to identify microRNA-423-5p. To that end, for the opening of a new horizon to the identification of micro-RNA-423-5p in human saliva samples a DNA-based biosensor was developed for the sensitive and specific monitoring of this biomarker by oligonucleotide hybridization strategy. For this purpose, the surface of a glassy carbon electrode (GCE) was automatically altered by poly (CS) utilizing the electropolymerization process to create a high-potential capturing layer. KCC-1-nPr-NH-Arg was utilized to increment of surface-to-volume toward increase of DNA loading on surface of electrode.

In summary, an efficient substrate for the appropriate and stable immobilization of probe-DNA was prepared and utilized to recognition of microRNA-423-5p using hybridization approach. Numerous important parameters, such as the hybridization duration and the concentration of micro-RNA-423-5p, were examined throughout the construction stages of the built genosensor analysis. Later, microRNA-423-5p in human actual samples was determined using electrochemical methods such as differential pulse voltammetry (DPV) and cyclic voltammetry (CV). The stability, reproducibility, and applicability of the biosensor for collecting saliva and using in plasma samples were evaluated as performance criteria.

2 Experimental

2.1 Chemicals and reagents

Bovine serum albumin (BSA), silver nitrate ($AgNO_3$), hydrogen peroxide (H_2O_2, 30 wt%), tri-sodium citrate (TSC) ($Na_3C_6H_5O_7$), polyvinyl pyrrolidone (PVP K-30), potassium ferricyanide $K_3Fe(CN)_6$, potassium ferrocyanide $K_4Fe(CN)_6$, and sulfuric acid (98%), were purchased from Sigma-Aldrich. The Chitosan (CS) solution was made by dissolving 0.005 gr of CS in a 0.1 M acetic acid solution (pH = 5). Phosphate-buffered saline (PBS) solutions with a concentration of 0.05 M and pH 7.4 was standard prepared by dissolving Na_2HPO_4 (0.1 M) and NaH_2PO_4 (0.1 M) in deionized water.

Table 1 summarized oligonucleotide sequences of DNA probe, microRNA-423-5p (target), 1-base mismatch, non-complement that purchased from Bioneer Co., Korea.

Table 1 Oligonucleotide sequences of DNA probe, microRNA-423-5p (target), 1-Base mismatch, non-complement

Type of DNA/RNA sequence	Sequences (5′ → 3′)
MicroRNA-423-5p	UGAGGGGCAGAGAGCGAGACUUU
DNA probe	5′-SH-TGTCTCCCCGGTGTCTGGCTCGA-3′
1-Base mismatch	TGGCTCCCCGGTGTCTGGTTCGA
Non-complement (MicroRNA-21)	TGTCGGGTTGCTGTCCTCTTC

The Faculty of Dentistry at Tabriz University of Medical Science, Iran, provided human saliva samples (Ethic code: IR.TBZMED.REC.1403.085). Also, human plasma samples were obtained from Tabriz University of Medical science, Tabriz, Iran, (ethic code: IR.TBZMED.REC.1403.085). All experiments were performed in accordance with the guide lines of institute (Tabriz University of Medical science), and approved by the ethics committee at Tabriz University of Medical science, Tabriz, Iran. Informed consents were obtained from human participants of this study.

Saliva sample of patients were taken when the subjects were fasting (at least 8 hours had elapsed since the previous meal and drink). Phosphate buffer (0.1 M) at pH = 7.4 was used for 30 seconds to cleanse the mouth cavity to guarantee cleanliness before sampling. 20 seconds of deionized water rinsing followed by the removal of the phosphate buffer from the mouth cavity. Following verification of the samples' clarity and lack of suspended particles, saliva was finally collected and utilized.

2.2 Electropolymerization of CS on the surface of the GCE

CS is commonly employed in the fabrication of biosensors because of its unique characteristics, including strong adhesion, lack of toxicity, high permeability, affordability, resistance to chemical alteration, ability to form thin films effectively, and capacity for electron transfer in reaction compounds due to its hydrophilic nature when swollen. In addition, CS may be used as a dispersant to create a durable polymeric film on the surfaces of different substrates.[33] CS was electropolymerized on pre-cleaned GCE electrode by using CV technique. In this regards, 20 cycles by CV technique within a potential range of −0.6 to +1.3 V was used for the electropolymerization CS. Fig. S1 (SI) displays the CV acquired from the electropolymerization of CS on the CGE.

2.3 Synthesis and characterization of KCC-1-nPr-NH-Arg and triangular silver nanoprism (TA-AgNPr)

The synthesis procedure of KCC-1-nPr-NH-Arg was done based on our pervious report.[34] Then, 1 mg of KCC-1-nPr-NH-Arg was dissolved in 100 mM of buffer solution and incubated in darl place at 37 °C for 24 hours. After that, the mixture was centrifuged for five minutes at 6000 rpm. After that, the supernatant was discarded. Subsequently, 5 μL of the suggested DFNS was drop-cast over the GCE-P(CS) surface and incubated for 6 hours at 4 °C. Lastly, GCE modified by P(CS)-KCC-1-nPr-NH-Arg dried at room temperature and utilized for the appropriate of probe DNA on the biosensor fabrication process. AgNPrs was synthesized and characterized according to our pervious report.[35]

2.4 Fabrication of genosensor

The preparation procedure for the developed biosensor substrate (GCE/P(CS)/KCC-1-nPr-NH-Arg/AgNPs) involves the electropolymerization of CS, modification of GCE/P(CS) with Ag nanoparticles in combination with KCC-1-nPr-NH-Arg, and immobilization of a particular DNA sequence. To that end, specific pDNAs were immobilized on the surface of P(CS)-KCC-

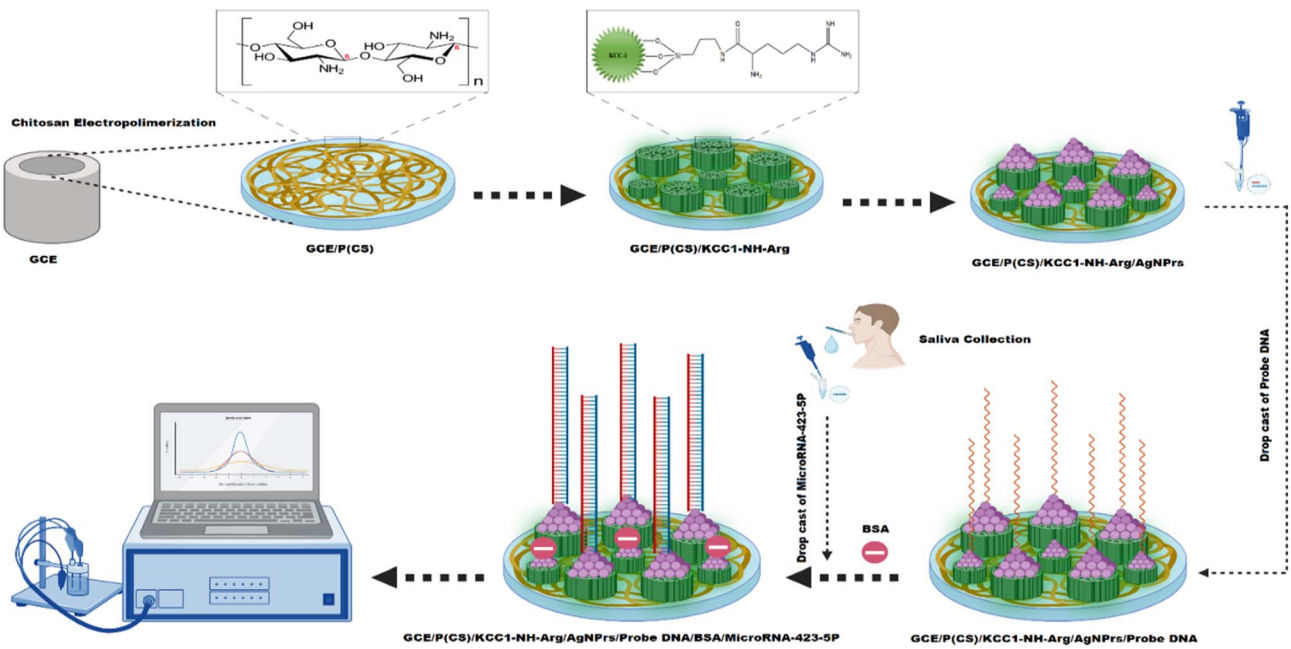

Scheme 1 The designed label-free electrochemical DNA based biosensor for detection microRNA-423-5p.

1-nPr-NH-Arg-AgNPs modified GCE. The immobilization process took place for 12 hours at 4 °C, which had been determined as the optimal incubation period. The P(CS)-KCC-1-nPr-NH-Arg-AgNPs-probeDNA was treated with 10 μL of BSA, a potent blocking agent, for 30 minutes at 25 °C to prevent binding to non-specific sites on the electrode. Finally, the modified GCE was subjected to 10 μL of microRNA-423-5p for 30 minutes at 37 °C. Scheme 1 illustrates the various stages of the genosensor fabrication process.

3 Results and discussion

3.1 Characterization of different steps of sensor fabrication using FE-SEM and EDX

The electrode surface was characterized at different stages of biosensor fabrication using FE-SEM and EDX techniques. FE-SEM images of electrodes in different modification states were recorded simultaneously. Fig. S2A (SI) depicts the FE-SEM image of GCE-P(CS), revealing the creation of P(CS) with a structured and organized architecture. Due to the presence of amine groups, CS is susceptible to oxidation and may readily form a polymer film by establishing covalent bonds (C–N) between the amine groups of CS and carbon electrodes. Also, Fig. S2B (SI) depicts the FE-SEM image of KCC-1-nPr-NH-Arg even out on the GCE-P(CS) surface. The electrode surface changes morphology, resembling the emergence of mushrooms from the surface. This verifies the effective formation of KCC-1-nPr-NH-Arg on the electrode surface. In addition, Fig. S2C (SI) indicated an FE-SEM image of the formation of Ag nanoparticles with prism morphology on the surface of the electrode. Fig. S2D (SI) shows an FE-SEM image obtained after immobilizing a particular DNA sequence containing a thiol group onto the surface of a GCE that has been coated with Ag nanoparticles. The surface of the electrode has become spongy after immobilizing the particular sequence containing the thiol group and establishing a connection between the thiol group and the Ag nanoparticles. Fig. 2E (SI) illustrate the FE-SEM image of the GCE that has been modified with P(CS)-KCC-1-nPr-NH-Arg-AgNPs. These images were taken after the DNA sequence had hybridized with the complementary sequence of the target (microRNA-423-5p). The effective interaction between DNA and the target analyte indicates the accomplishment of the genosensor manufacturing process. Furthermore, the analysis of the electrode using EDX confirms the effective creation of the genosensor after several manufacturing procedures (Fig. S3 (SI)).

3.2 Electrochemical behavior of the designed genosensor

The electrochemical performance of the developed genosensor was evaluated using CV and DPV techniques. To verify the accuracy of the biosensor production procedure, CVs was recorded in the potential range of −1 to +1 V. Voltammograms were obtained and compared after each step of electrode construction (Fig. 1A).

Also, Fig. 1B illustrates the peak histogram of peak currents *versus* type of electrode. As can be seen, applying a coating of poly-CS to the surface of the GCE results in a modest decrease in the anodic peak current, reducing it from 25 to 15.49 μA. Subsequently, by introducing KCC-1-nPr-NH-Arg onto the electrode surface, the anodic peak current's magnitude escalates as a result of arginine's presence on the DFNS structure and its contact with the surface, ultimately reaching a numerical value of 38.11 μA. Despite the polymer's inhibitory effect on electron transfer, the numerous functional groups on the surface of this bioactive polymer, such as amine, methyl, and hydroxyl groups,

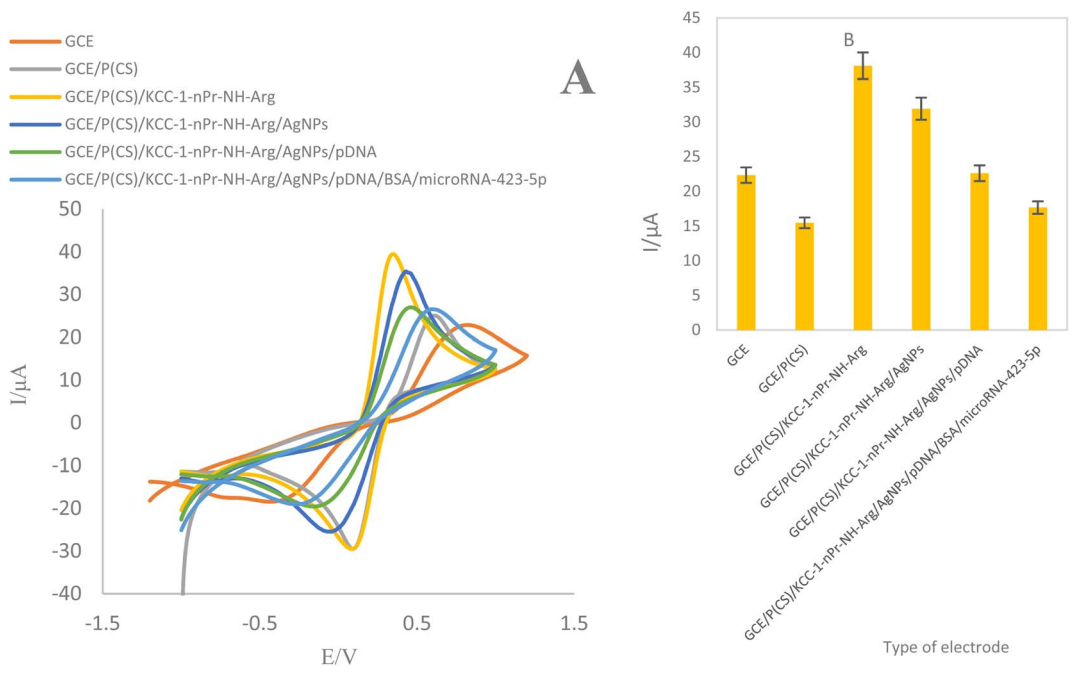

Fig. 1 (A) CVs of electrodes in the presence of Ferro/Ferri solution. (B) Histogram of peak current *versus* type of electrodes.

enable the introduction of suitable substrates for binding with KCC-1-nPr-NH-Arg. Despite the high conductivity of applied metal nanoparticles (AgNPs), due to the encapsulation of Ag nanoprism into the porous structure of KCC-1-nPr-NH-Arg, the anodic peak current has been decreased and reached 31.93 μA.

Subsequently, the electrode's peak current, which was modified with the probe DNA, experienced a notable decrease and reached 22.61 μA. This was caused by the uneven buildup of the thiolated probe on the electrode's surface. According to obtained results, the presence of the electroactive compound $Fe(CN)_6^{-3/-4}$ on the surface of sensor led to increment of the peak current sensor. Subsequently, after hybridization of DNA with microRNA-423-5p a significant decrease was accrued in the anodic peak currents associated with the redox state of $Fe(CN)_6^{-3/-4}$. The reduction in the peak current of anodic condition served as a reliable indicator of the successful execution of the DNA hybridization. The hybridization procedure may be carried out using a modified electrode that incorporates a self-arranged single-strand probe. The decrease in anodic and cathodic peak current intensity in the voltammograms can be attributed to the immobilization of ssDNA probes and the accumulation of dsDNA. This decrease is caused by the presence of the electroactive anionic compound $Fe(CN)_6^{-3/-4}$, which also carries a negative charge. Consequently, the current's strength diminishes, leading to a significant decrease in the oxidation peak of $Fe(CN)_6^{-3/-4}$. Reduction in the anodic peak current of CVs is evident that dens-loading of DNA was increased and led to steric hindrance and the negative charge of the DNA. Therefore, the redox potentials were shifted to positive values.

The DPV procedure precisely aligns with the result derived from CV, yielding the following outcomes. Fig. S4A(SI) shows DPVs of biosensor in different fabrication steps. By electropolymerization of the P(CS), the peak current reached to 16.43 μA. Adding mesoporous nano-silica further increased the peak current to 48.33 μA. However, the encapsulation of Ag nanoprism into the porous structure of KCC-1-nPr NH-Arg decreased the peak current to 20.58 μA. Finally, after introducing microRNA-423-5p, the I_p was dropped to 8.48 μA and confirmed hybridization process.

3.3 Analytical studies

The DPV technique was used to determine the target microRNA-423-5p after hybridization with probe DNA. Following the modification of the electrode surface, a volume of 5 μL containing a single-strand DNA probe at a concentration of 5 nM was applied to the electrode surface to achieve hybridization with microRNA-423-5p. The aforementioned procedures were executed for the concentration (1, 0.05, 0.01, and 0.001 nM) of a single-stranded analyte (microRNA-423-5p). Fig. 2 shows DPV and obtained calibration curve of genosensor.

The findings indicate a direct correlation between the peak current of the calibration curve and the varying Napierian Logarithm of microRNA-423-5p concentration. Therefore, it is feasible to identify a reduced amount of microRNA-423-5p in standard samples. The constructed biosensor has shown the capability to detect the presence of microRNA-423-5p in standard solution.

3.3.1 Analytical studies in real samples (human blood plasma). For this purpose, a blood sample was obtained from a 30 year-old person who is in good health and does not have cancer. The blood was collected in a tube without any additives and left to coagulate for 60 minutes at room temperature. This

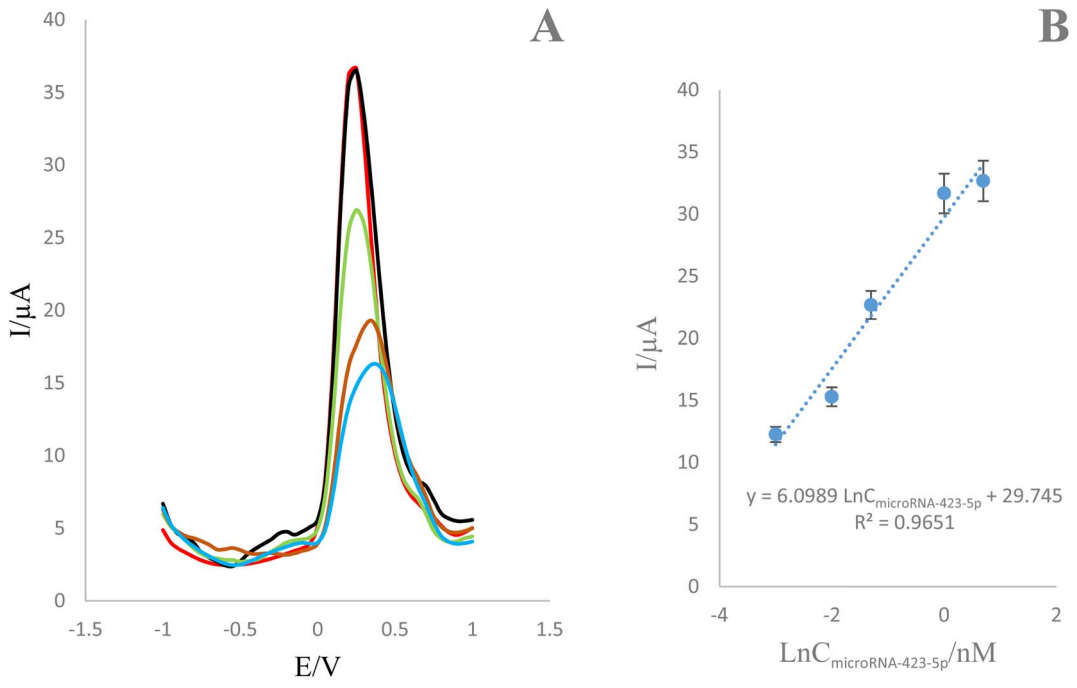

Fig. 2 (A) DPVs of genosensor incubated in the presence of different concentrations of microRNA-423-5p: 5, 1, 0.05, 0.01, 0.001 nM in 0.01 M $Fe(CN)_6^{-3/-4}$ and 0.01 M KCl as the supporting electrolyte (B) calibration curve.

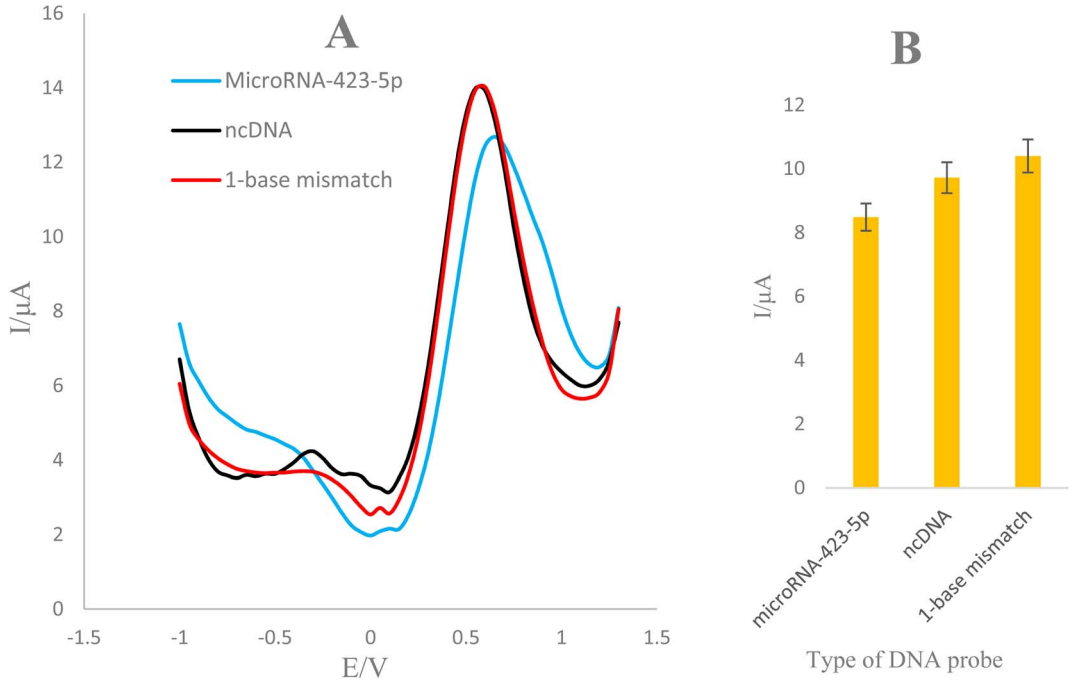

Fig. 3 (A) DPVs of the genosensor in the presence of microRNA-423-5p, ncDNA, and 1-base mismatch sequences. (B) Histogram of peak current *vs.* to different types of DNA sequences.

process was done to separate the serum from the rest of the blood. Subsequently, it was kept overnight at a temperature of 4 °C. The samples underwent two rounds of centrifugation, first with a force of 150 g for 5 minutes, followed by a subsequent round for 15 min. Subsequently, the tubes were often subjected to rotation, the samples were divided into equivalent pieces, and they were stored at a temperature of −20 °C.

To assess the impact of various concentrations of microRNA-423-5p in actual human plasma samples, microRNA-423-5p was added to human plasma at a ratio of 1 : 1 (V/V). The mixture was then placed on the surface of the designed electrode (GCE/P(CS)/KCC-1-nPr-NH-Arg/AgNPs/probeDNA) and incubated. DPVs of genosensor were recorded in the existence of different concentrations of microRNA-423-5p (0.001, 0.005, 0.01, 0.05, and 0.1 nM) spiked in human plasma samples (Fig. S5A (SI)).

According to the obtained results (Fig. S5B (SI)) the regression equation in the range of 0.001 to 0.1 nM is as follows:

$$I(\mu A) = 171.52\ C_{\text{microRNA-423-5p}} + 29.74,\ R^2 = 0.9381$$

Its sensitivity is 171.52 μA nM^{-1} with LLOQ = 1pM.

According to obtained results, sensing of microRNA-423-5p in real samples by designed substrate is possible.

3.3.2 Analytical study. To illustrate utilization of biosensor toward non-invasive monitoring of microRNA-423-5p, DPVs were recorded. So, the DPV technique was chosen as a sensitive diagnostic method for detecting microRNA-423-5p in healthy human saliva samples. Real unprocessed human saliva samples were used to for the early-stage identification of oral cancer.

Saliva samples were obtained during the fasting period, which required a minimum of 8 hours from the last use of food and beverages. To guarantee oral cavity cleanliness prior to sampling, a phosphate buffer solution (0.1 M) with a pH of 7.4 was used to rinse the oral cavity for a duration of 30 seconds. Following the removal of the phosphate buffer, the oral cavity was flushed with deionized water for a duration of 20 seconds. Ultimately, saliva samples were gathered and used only after confirming their transparency and lack of suspended matter (Fig. S6).

The regression equation in the range of 0.01 to 1 nM is as follows:

$$I(\mu A) = 6.0081\ C_{\text{microRNA-423-5p}} + 8.2013,\ R^2 = 0.9641$$

Its sensitivity is 6.0081 μA nM^{-1} with LLOQ = 0.01 nM.

The findings indicate a direct correlation between the peak current of the calibration curve and the varying concentration of microRNA-423-5p. It is feasible to identify a reduced amount of microRNA-423-5p in real samples. The constructed biosensor has shown the capability to detect the presence of microRNA-423-5p in real samples (human saliva sample).

Table 2 RSD of (5, 1, 0.1, 0.05 nM) concentrations of the target analyte (microRNA-423-5p) to check the repeatability of the sensor

	5 nM	1 nM	0.1 nM	0.05 nM
	28.93188	31.74284	31.84005	35.951511
	23.14671	26.10715	27.06153	31.827472
	18.21012	21.26441	23.32687	27.924419
Average	23.42957	26.37147	27.40948	31.901134
SD	**5.366473**	**5.244216**	**4.267245**	**4.0140531**

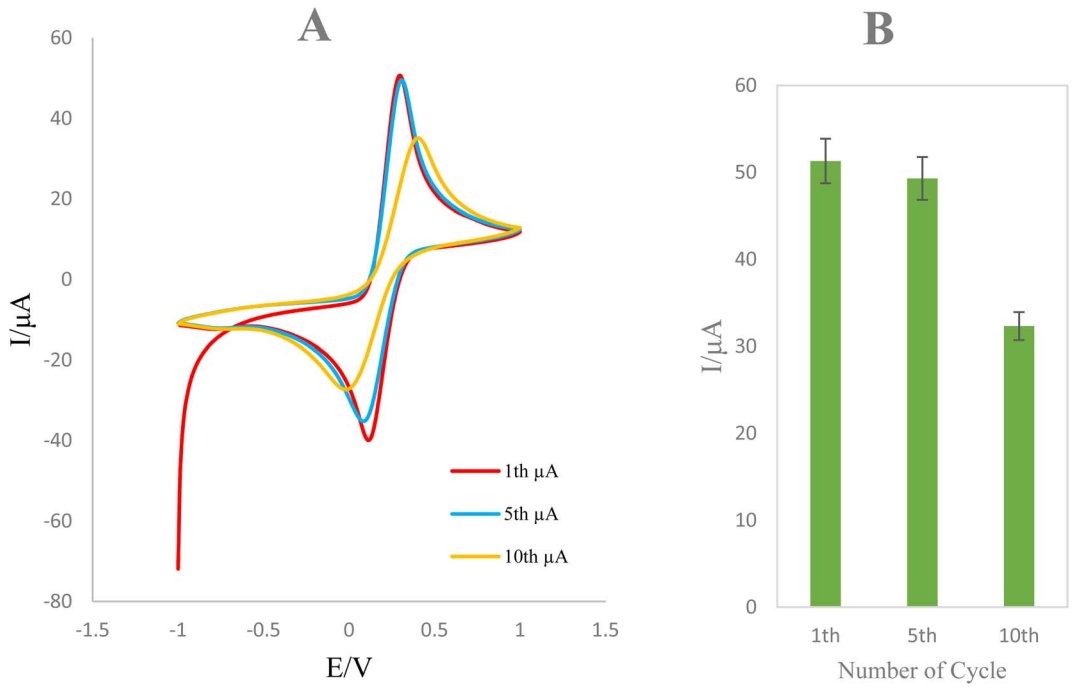

Fig. 4 (A) CVs of P(CS)/KCC-1-nPr-NH-Arg modified GCE in the potential range of −1 to 1 and sweep rate of 0.1 V s^{-1} in different cycle numbers (1,5 and 10). (B) Histogram of peak current *vs.* number of cycles.

3.4 Analytical validation

3.4.1 Selectivity of the genosensor. DPVs techniques were used to analyses the selectivity of the biosensor by using a ncDNA and 1-base mismatch to compare the selectivity of bioreceptor to target analyte (microRNA-423-5p) sequences in standard solution (Fig. 3).

At this stage, due to the overlapping of sequence ncDNA and 1-base mismatch, we used variation of peak current to interpret the data of microRNA-423-5p. In this direction, sequence microRNA-423-5p had a current intensity of 8.48 μA and sequences ncDNA and 1-base mismatch had a current intensity of 9.71 and 10.39 μA, respectively. In this way, the designed biosensor has selectivity for microRNA-423-5p.

3.4.2 Repeatability of the biosensor. The repeatability of a biosensor is a crucial metric for assessing its performance. Repeatability pertains to the ability of a biosensor to provide consistent responses when subjected to similar experimental conditions. For the assessment of biosensor repeatability, DPVs of the developed genosensor was recorded using 0.01 M $Fe(CN)_6^{-3/-4}$ and 0.01 M KCl as the supporting. (Fig. S7(SI)). Accuracy refers to the degree of closeness between the results received from a procedure after several repeats. It is quantified by the percentage of relative standard deviation (%RSD). A RSD of up to 15% is deemed acceptable for biological samples by the FDA (Food and Drug Administration) standard.

%RSD = Standard deviation (SD)/average of detection values (Mean).

All measurements were conducted in triplicate, and the error bars show the RSD% range of 4–5 for the measurements. This indicates the high accuracy of the genosensor (Table 2).

The low value of the RSD found indicates the ideal repeatability of the current biosensor, hence confirming its efficacy in providing consistent results across various samples. Furthermore, the simplicity and reproducibility of the biosensor fabrication process are significant and beneficial benefits.

3.4.3 Evaluation of the stability. Continuous monitoring is necessary to ensure the stability, which is a crucial aspect of biosensors' function. Stability refers to the extent to which biosensors are prone to internal and external environmental risks.

3.4.3.1 Intra-day surface stability. To assess the intra-day stability of the internalization of the GCE surface, the durability of the matrix, P(CS)/KCC-1-nPr-NH-Arg modified GCE, was evaluated at 30 minute intervals over four hours (Fig. S8(SI).

For this purpose, CVs of electrode (without existence of biological element (probe DNA)) exhibited a steady oscillation and maintained a value of around 50 μA for a duration of up to three hours. Starting with the third hour, the electrode lost its stability and achieved a value of 45 μA, indicating the three-hour stability of the electrode surface. Hence, once the production of this genosensor is completed, it should be promptly deployed.

3.4.3.2 Inter-Day surface stability. To assess the Inter-Day stability of the electrode surface internalization over a period of two days, we evaluated the P(CS)/KCC-1-nPr-NH-Arg modified GCE matrix's durability (Fig. S9(IS)). The matrix initially exhibited stability on the first day, with a current intensity of around 50 μA. However, it subsequently experienced a significant reduction and reached to 7 μA on second day.

3.4.4 Cyclic stability of sensor substrate. CVs of P(CS)/KCC-1-nPr-NH-Arg modified GCE was recorded in 10 consecutive cycles (Fig. 4). This was done to assess the stability of the matrix

on the electrode surface during repeated measurements, which might serve as an indicator of the genosensor's stability. During the first five cycles, the peak current showed a consistent fluctuation and remained around 50 μA. However, by the 10th cycle, there was a sudden drop to 32.31 μA. Therefore, it can be concluded that the modified electrode biosensor substrate delivers the best results for up to 5 uses.

4 Conclusion

In summary, an innovative label-free electrochemical genosensor was developed for the sensitive and specific recognition of microRNA-423-5p. For the first time, DNA hybridization approach was utilized for the monitoring of target biomarker of OC in human biofluids. Also, by developed biosensor a non-invasive analysis of microRNA-423-5p was performed in human saliva samples in the linear range of 1 pM to 5 nM. Novel type of materials like KCC-1-npr-NH-Arg, TA-AgNPs, and P(CS) were utilized for the construction of this biodevice. Finally, using engineered bioanalytical sensor, specific detecting of microRNA-423-5p was performed in the presence of interfering specious including ncDNA and mismatch-DNA. Constructed biosensor provide significant advantages, making them a viable electrochemical device for detecting microRNA-423-5p in human biofluids. This opens up new possibilities for the early-stage detection of OC.

Conflicts of interest

There are no conflicts to declare.

Data availability

The data supporting this article is included within the manuscript and as part of the supplementary information (SI). Supplementary information: Fig. S1: CVs of GCE in the present of CS solution (0.005 gr in 0.1 M acetic acid) in the scan rate = 100 mV s^{-1}; number of cycles = 20. Fig. S2: FE-SEM images of (A) P(CS), (B) P(CS)-KCC-1-nPr-NH-Arg, (C) P(CS) KCC-1-nPr-NH-Arg-AgNPs, (D) P(CS)-KCC-1-nPr-NH-Arg-AgNPs-probeDNA, (E) P(CS)-KCC-1-nPr-NH-Arg-AgNPs-probeDNA-BSA-MicroRNA-423-5p in different magnifications. Fig. S3: EDS spectra of fabricated genosensor. Fig. S4: (A) DPVs of bare GCE, P(CS)-modified GCE, P(CS)-KCC-1-nPr-NH-Arg-modified GCE, P(CS)-KCC-1-nPr-NH-Arg-AgNPs-modified GCE, P(CS)-KCC-1-nPr-NH-Arg-AgNPs-probeDNA-modified GCE, P(CS)-KCC-1-nPr-NH-Arg-AgNPs-probeDNA-BSA-microRNA-modified GCE in 0.01 M $Fe(CN)_6^{-3/-4}$ and 0.01 M KCl as the supporting electrolyte with a sweep rate of 100 mV s^{-1}. (B) Bar-graph of changes in peak current at different stages of genosensor fabrication. Fig. S5: (A) DPVs of the genosensor in different concentrations of microRNA-423-5p: 0.1, ,0.05, 0.01, 0.005, 0.001 nM with treated human plasma sample in the present of 0.01 M $Fe(CN)_6^{-3/-4}$ and 0.01 M KCl as the supporting electrolyte. (B) Calibration curve against the concentration value microRNA-423-5p. Fig. S6: (A) DPVs of the constructed genosensor in the present of different concentrations of microRNA-423-5p: 0.01,0.05, 1 nM with healthy human saliva samples in 0.01 M $Fe(CN)_6^{-3/-4}$ and 0.01 M KCl as the supporting electrolyte. (B) Calibration curve of biosensor *versus* the amount of microRNA-423-5p. Fig. S7: (A–D) DPVs of genosensor recorded for repeatability of 5, 1, 0.1 and 0.05 nM concentrations in 0.01 M $Fe(CN)_6^{-3/-4}$ and 0.01 M KCL as the supporting electrolyte. (B) Histogram of peak current *vs.* different concentrations of microRNA-423-5P sequences in 3 repetitions. Fig. S8: (A) CVs of P(β-CD)/KCC-1-nPr-NH-Arg-modified GCE in the potential range of −1 to 1 and sweep rate of 0.1 V s^{-1} in the presence of 0.01 M $Fe(CN)_6^{-3/-4}$ and 0.01 M KCL as the supporting electrolyte in different time of incubation. (B) Histogram of peak current *vs.* time of incubation. Fig. S9: (A) CVs of P(β-CD)/KCC-1-nPr-NH-Arg-modified GCE in the potential range of −1 to 1 and sweep rate of 0.1 V s^{-1} in the presence of 0.01 M $Fe(CN)_6^{-3/-4}$ and 0.01 M KCL as the supporting electrolyte in different time of incubation. (B) Histogram of peak current *vs.* period time of detection. Fig. S10: (A) CVs of GCE/P(CS)/KCC-1-nPr-NH-Arg/AgNPs in the process of $[Fe(CN)_6]^{3-/4-}$ solution in diverse sweep rates (0.15, 0.1, 0.09, 0.07, 0.06, 0.05, 0.04, 0.03, 0.02, 0.01, 0.005, 0.002 mV/s); (B) variation of I_p *vs.* v; (C) variation of I_p *vs.* $v^{0.5}$; (D) variation of I_p *vs.* ln$v$; (E) the plot of Napierian logarithm of oxidation peak current *vs.* Napierian logarithm of sweep rates. See DOI: https://doi.org/10.1039/d5ra07098h.

Acknowledgements

This work was supported by Tabriz University of Medical Sciences (74167).

References

1 S. Dixit, A. Kumar and K. Srinivasan, *Diagnostics*, 2023, **13**, 1353.
2 J. Balakittnen, C. E. Weeramange, D. F. Wallace, P. H. Duijf, A. S. Cristino, L. Kenny, S. Vasani and C. Punyadeera, *Wiley Interdiscip. Rev.:RNA*, 2023, **14**, e1754.
3 S. A. Mosaddad, R. A. Namanloo, S. S. Aghili, P. Maskani, M. Alam, K. Abbasi, F. Nouri, E. Tahmasebi, M. Yazdanian and H. Tebyaniyan, *Med. Oncol.*, 2023, **40**, 91.
4 T. Flügge, R. Gaudin, A. Sabatakakis, D. Tröltzsch, M. Heiland, N. van Nistelrooij and S. Vinayahalingam, *Sci. Rep.*, 2023, **13**, 2296.
5 J. Bouaoud, P. Bossi, M. Elkabets, S. Schmitz, L. C. van Kempen, P. Martinez, S. Jagadeeshan, I. Breuskin, G. J. Puppels and C. Hoffmann, *Cancers*, 2022, **14**, 1815.
6 C.-C. Yang, Y.-F. Su, H.-C. Cheng, Y.-C. Juan, Y.-W. Chiu, C.-H. Wu, P.-Y. Chen, Y.-H. Lee, Y.-L. Chen and Y.-T. Chen, *Diagnostics*, 2022, **12**, 1544.
7 S. Warnakulasuriya and A. Kerr, *J. Dent. Res.*, 2021, **100**, 1313–1320.
8 Y.-F. Su, Y.-J. Chen, F.-T. Tsai, W.-C. Li, M.-L. Hsu, D.-H. Wang and C.-C. Yang, *Diagnostics*, 2021, **11**, 1287.
9 D. Chakraborty, C. Natarajan and A. Mukherjee, *Adv. Clin. Chem.*, 2019, **91**, 181–200.
10 P.-H. Chen, H.-Y. Lee, Y.-F. Chen, Y.-C. Yeh, K.-W. Chang, M.-C. Hou and W.-C. Kuo, *Cancers*, 2020, **12**, 2376.
11 M. DeCoro and P. Wilder-Smith, *Expet Rev. Anticancer Ther.*, 2010, **10**, 321–329.

12 A. E. Heidari, S. P. Sunny, B. L. James, T. M. Lam, A. V. Tran, J. Yu, R. D. Ramanjinappa, K. Uma, P. Birur and A. Suresh, *IEEE J. Sel. Top. Quantum Electron.*, 2018, **25**, 1–8.
13 Q. Xiong, Y. Zhang, J. Li and Q. Zhu, *Genes*, 2022, **13**, 2072.
14 M. Eslami, S. Khazeni, X. M. Khanaghah, M. H. Asadi, M. A. Ansari, J. H. Garjan, M. H. Lotfalizadeh, M. Bayat, M. Taghizadieh and S. P. Taghavi, *Cancer Cell Int.*, 2023, **23**, 182.
15 Z. Xu, X. Li, L. Pan, R. Tan, P. Ji and H. Tang, *J. Oral Pathol. Med.*, 2022, **51**, 358–368.
16 S. Dey, B. Biswas, A. Manoj Appadan, J. Shah, J. K. Pal, S. Basu and S. Sur, *Cancers*, 2023, **15**, 3752.
17 L. Zhang, M. Wang, W. Ren, S. Li, K. Zhi, L. Gao and J. Zheng, *Oral Dis.*, 2023, **29**, 1439–1453.
18 S. Gupta, P. Kumar, J. Maini, B. Das and M. Bhardwaj, *J. Cancer Sci. Ther.*, 2019, **11**, 086–090.
19 Ó. Rapado-González, R. López-López, J. L. López-Cedrún, G. Triana-Martínez, L. Muinelo-Romay and M. M. Suárez-Cunqueiro, *Cells*, 2019, **8**, 1653.
20 S. Yete and D. Saranath, *Oral Oncol.*, 2020, **110**, 105002.
21 T. Nonaka and D. T. Wong, *Annu. Rev. Anal. Chem.*, 2022, **15**, 107–121.
22 A. I. Mäkinen, V. Y. Pappalardo, M. J. Buijs, B. W. Brandt, A. A. Mäkitie, J. H. Meurman and E. Zaura, *Microbiome*, 2023, **11**, 171.
23 A. P. Ahrens, D. E. Sanchez-Padilla, J. C. Drew, M. W. Oli, L. F. Roesch and E. W. Triplett, *Sci. Rep.*, 2022, **12**, 14306.
24 L. B. Smith, A. C. Chagas, I. Martin-Martin, J. M. Ribeiro and E. Calvo, *Insect Biochem. Mol. Biol.*, 2023, **153**, 103898.
25 M. Martorella, S. Kasela, R. Garcia-Flores, A. Gokden, S. E. Castel and T. Lappalainen, *BMC Genom.*, 2023, **24**, 790.
26 G. Riccardi, M. G. Bellizzi, I. Fatuzzo, F. Zoccali, L. Cavalcanti, A. Greco, M. d. Vincentiis, M. Ralli, M. Fiore and C. Petrella, *Proteomes*, 2022, **10**, 37.
27 L. F. B. Miranda, C. V. Lima, R. Pagin, R. C. Costa, M. M. A. Pereira, E. D. de Avila, M. Bertolini, B. Retamal-Valdes, J. A. Shibli and M. Feres, *J. Proteome Res.*, 2023, **22**, 857–870.
28 E. Martina, A. Campanati, F. Diotallevi and A. Offidani, *J. Clin. Med.*, 2020, **9**, 466.
29 M. Hasanzadeh, N. Shadjou and M. de la Guardia, *TrAC, Trends Anal. Chem.*, 2017, **91**, 125–137.
30 P. Dongiovanni, M. Meroni, S. Casati, R. Goldoni, D. V. Thomaz, N. S. Kehr, D. Galimberti, M. Del Fabbro and G. M. Tartaglia, *Int. J. Oral Sci.*, 2023, **15**, 27.
31 C. Romani, E. Salviato, A. Paderno, L. Zanotti, A. Ravaggi, A. Deganello, G. Berretti, T. Gualtieri, S. Marchini and M. D'Incalci, *Theranostics*, 2021, **11**, 2987.
32 A. J. Bowers, X. Zhou and J. Ed, *J. Educ. Stud. Placed A. T. Risk*, 2019, **24**, 20–46.
33 S. Hassanpour, A. Saadati and M. Hasanzadeh, *J. Mol. Recognit.*, 2020, **33**, e2817.
34 N. Hasannezhad and N. Shadjou, *J. Mol. Recognit.*, 2022, **35**, e2956.
35 A. Saadati, F. Farshchi, M. Hasanzadeh and F. Seidi, *Anal. Methods*, 2021, **13**, 3909–3921.